Minimization of bauxite residue neutralization products using nanofiltered seawater

Sara J. Couperthwaite[1*], Dean W. Johnstone[1], Mark E. Mullett[2], Kelvin J. Taylor[2], and Graeme J. Millar[1]

[1)] Chemistry, Physics, Mechanical Engineering, Science and Engineering Faculty, Queensland University of Technology, GPO Box 2434, Brisbane Queensland 4001, Australia.
Fax: +61 7 3138 1804; Tel +61 7 3138 4766; E-mail: sara.couperthwaite@qut.edu.au
[2)] Hatch Associates Pty Ltd, 144 Stirling Street, Perth, WA 6000, Australia

Abstract

Currently, open circuit Bayer refineries pump seawater directly into their operations to neutralize the caustic fraction of the Bayer residue. The resulting supernatant has a reduced pH and is pumped back to the marine environment. This investigation has assessed modified seawater sources generated from nanofiltration processes to compare their relative capacities to neutralize bauxite residues. An assessment of the chemical stability of the neutralization products, neutralization efficiency, discharge water quality, bauxite residue composition, and associated economic benefits have been considered to determine the most preferable seawater filtration process based on implementation costs, savings to operations and environmental benefits. The mechanism of neutralization for each technology was determined to be predominately due to the formation of Bayer hydrotalcite and calcium carbonate, however variations in neutralization capacity and efficiencies have been observed. The neutralization efficiency of each feed source has been found to be dependent on the concentration of magnesium, aluminium, calcium and carbonate. Nanofiltered seawater with approximately double the amount of magnesium and calcium required half the volume of seawater to achieve the same degree of neutralization. These studies have revealed that multiple neutralization steps occur throughout the process using characterization techniques such as X-ray diffraction (XRD), infrared (IR) spectroscopy and inductively coupled plasma optical emission spectroscopy (ICP-OES).

Keywords: nanofiltration, bauxite residue, red mud, Bayer process, seawater neutralization

1. Introduction

One of world's greatest industrial waste streams belongs to the alumina industry (bauxite residue – red mud), which is estimated to have generated around 3 billion tonnes of residue globally (2010) with an additional 120 million tonnes per annum continuing to be produced.[1-3] The magnitude of waste being generated by this industry clearly demonstrates the need for future developments in not only responsible disposal methods but also technologies that reduce the production of waste through the optimization of operation processes or re-use the waste for beneficial purposes. Bauxite residue is produced by the Bayer process, which involves the digestion of bauxite ore using highly caustic solutions at elevated temperatures and pressures to form a solution of sodium aluminate and an insoluble residue (red mud). There are a number of factors that influence the quantity of bauxite residue that is produced: 1) aluminium content in the ore, 2) type of aluminium oxide/hydroxide, 3) temperature and pressure conditions. The Bayer process can produce between 0.3 and 2.5 tonnes of caustic red mud waste for every tonne of alumina produced[2]. Red mud is classified as a "hazardous material" under the Basel Convention.[4] Due to the complexity and classification of bauxite residue, numerous researchers from a variety of fields are trying to utilise the waste residue to minimize environmental impacts caused by tailings dams and the associated costs of storage facilities (more than $80 million a year).[5] Some of the more current research focuses on remediation,[6-9] adsorbents[10-14] and metal recovery[15-17].

Apart from the visible implications of storing bauxite residue in large tailings dams, these residues are highly alkaline and contain an array of inorganic and organic species with potentially harmful environmental effects. Bauxite residue (which is usually in the form of slurry) is mainly comprised of iron oxides, titanium oxides, silicon oxides and undissolved alumina, along with a wide range of other oxides depending on the country of origin. Trace levels of metal oxides, such as arsenic, cadmium, chromium, copper, gallium, lead, mercury, nickel and in some cases thorium and uranium, are of particular concern.[18] The alkalinity of the residue exists in both solid and solution as: 1) entrained liquor (sodium hydroxide, sodium aluminate and sodium carbonate), 2) calcium compounds, such as hydrocalumite, tri-calcium aluminate and lime, and 3) sodalite ($(NaAlSiO_4)_6(Na_2X)$, where X can be SO_4^{2-}, CO_3^{2-}, $Al(OH)_4^-$ or Cl^-).[19] All of these compounds need to react with the neutralizing agent (seawater, mineral acids or carbon dioxide) to achieve "full" neutralization, however this is not achieved in normal operation conditions due to slow kinetic reactions involving calcium and silica compounds. There are two types of neutralization water management systems in the alumina industry:

1) Open-circuit: discharge of neutralized residue water to the environment (rivers, estuaries, marine waters) after clarification.
2) Closed-circuit: no discharge of residue water and requires the containment of residue in large tailings dams or is recycled to the refinery.

Current environmental management programs along coastal areas of Australia involve the neutralization of alumina wastewater through the addition of seawater, which produces a precipitate known as Bayer hydrotalcite ($Mg_6Al_2(OH)_{16}CO_3 \cdot 4H_2O$). Hydrotalcite is best visualised by starting with the structure of brucite (Figure 1A), and upon the substitution of Al^{3+} into the brucite structure, the layered hydrotalcite structure forms with intercalated anionic species (primarily carbonate and sulphate). The formation of hydrotalcite has a dual purpose in the neutralization process: 1) reduces the alkalinity of the entrained liquor in the residue and 2) removes metals, metalloids and anionic species. The seawater neutralization process reduces the alkalinity of the residue to safe limits for discharge into tailings dams and for reuse in a number of applications. Environmental Protection Agency discharge limits state that a pH range of 6-9 is generally acceptable, depending on the receiving water environmnet.[20] However, in order to achieve these limits up to 20 times the amount of seawater is required to neutralize an equivalent amount of bauxite residue.[19] This increases discharge volumes and the burden of the alumina industry on the environment.

The formation of hydrotalcite reduces the pH and soluble metals concentrations to the point where a clarified effluent (reacted seawater) can be discharged to the environment,[7, 21] while the residual slurry or filter cake is stored in large tailings dams. The disposal of numerous treated wastes into rivers, estuaries and marine waters is not uncommon, nevertheless, when the full array of anthropogenic wastes are taken into account it is inevitable that adverse effects will be observed in our water resources. Of particular concern is the release of metals and trace elements common in industrial waste streams,[22] which are known to cause skeletal deformities and various developmental abnormalities in marine fish.[23] New technologies and environmental management programs can mitigate the overall effect of effluent discharge on aquatic environments: however in all circumstances minimizing the amount of waste discharged will ensure the survival of these ecosystems.

The reactive species in seawater for the neutralization of bauxite residues are magnesium and calcium, therefore increasing the amount of these ions in seawater would reduce the overall volume required to achieve neutralization. Nanofiltration technology solves the problem of additional washing (waste reduction) due to nanofiltration membranes that allow mono-valent ions to pass through the membrane (such as sodium and chloride), while trapping divalent species in the retentate (magnesium and calcium). Thus, nanofiltration increases the reactivity of seawater while maintaining a salt content similar to that of the original seawater making it more suitable for land amelioration or remediation programs. It also significantly reduces the amount of neutralized water that is discharged into marine environments, improving the sustainability of the industry.

This study is an extension of the work previously conducted by Taylor *et al.* in 2011 which focused on the engineering aspects of using nanofiltered seawater.[24] Their aims were to determine the extent to which seawater could be concentrated using NF membranes before scaling commenced or before the osmotic pressure became excessive. In this study, a comparative reactivity of seawater and seawater NF concentrate has been undertaken to gain an understanding of the equipment capacities required and capital reduction benefits that could reasonably by anticipated by alumina refiners. This investigation focuses on the chemical processes involved and provides an assessment on the advantages of using nanofiltered seawater instead of seawater. The mineral composition, stability and mechanisms involved in the neutralization of Bayer liquor using seawater and nanofiltered seawater will be examined, followed by a statement on the environmental, social and economic implications of this technology on the alumina industry.

2. Materials and methods

Seawater was collected in southern Western Australia during July 2012 approximately 0.1 km off shore, which was pre-filtered using 5 μm cartridge filters. A portion of this seawater was then processed by nanofiltration in order to double the concentration of magnesium and calcium cations, while maintaining the same concentration for all other ions in seawater. Nanofiltered seawater was prepared using a 4" diameter spiral wound DK membrane from GE Power and Water at a constant pressure of 2500 kPa and flux of 30 Litre/m^2/h LMH. Cross flow filtration over a membrane surface under pressure was used to concentrate magnesium and calcium (61% recovery) by rejecting it to the retentate, while passing sodium chloride to the permeate. The recovery rate cannot generally exceed 65% due to the formation of calcium sulphate.

Synthetic seawater solutions were prepared from AR grade chemicals and 18.2MΩ water (Supporting Information 1).

Neutralization products were collected throughout the neutralization process in order to establish the mechanism and stability of precipitates. These experiments were conducted using a titration addition method, whereby seawater/nanofiltered seawater was added to 200mL of Bayer liquor (5.9g/L – Al_2O_3) at a molar ratio of 4.5:1. Details of the Bayer liquor composition are found in Supporting Information 2. A Watson and Marlow peristaltic pump was used to deliver seawater or nanofiltered seawater to 200mL of Bayer liquor at flow rate of 20mL/min and tubing diameter of 3.2mm. The resultant solution was stirred at 400rpm using a prop paddle (35mm diameter) and an IKA overhead stirrer. The pH was monitored at 30 second intervals using a TPS pH meter and Sentek general laboratory probe (calibrated using buffer 7 and 10). Samples (100mL) were extracted using a 50mL syringe as the pH reduced by a factor of 0.5 until a pH of 9.5 was reached. Samples were placed in a

250mL bottle and centrifuged using a Centurion Scientific C2 Series centrifuge for 5 minutes at 2500rpm. The liquid portion was transferred into a sample container, while the solid component was washed with 150mL of deionized H_2O before being centrifuged again. The solid component was placed in the oven overnight to dry (90°C) and then crushed to a fine powder using an agate ball mill.

X-Ray diffraction patterns were collected using a Philips X'pert wide angle X-Ray diffractometer, operating in step scan mode, with Co Kα radiation (1.7902 Å). Patterns were collected in the range 3 to 90° 2θ with a step size of 0.02° and a rate of 30s per step. Samples were prepared as Vaseline thin films on silica wafers, which were then placed onto aluminium sample holders. The Profile Fitting option of the software uses a model that employs twelve intrinsic parameters to describe the profile, the instrumental aberration and wavelength dependent contributions to the profile.

Solutions were analysed using a VISTA-MPX CCD simultaneous ICP-OES instrument that had been diluted by a factor of 2 using a Hamilton Diluter. A certified standard from Australian Chemical Reagents (ACR) containing 1000ppm of aluminium, calcium, magnesium, and sodium was diluted to form a multi-level calibration curve and an external reference that was used to monitor instrument drift and accuracy of the results obtained. Results were obtained using an integration time of 0.15 seconds with 3 replications. Wavelengths used were as follows: Al (396.152), Ca (422.673), Mg (285.213) and sodium (589.592).

Infrared spectra were obtained using a Nicolet Nexus 870 Fourier Transform infrared spectrometer (FTIR) with a smart endurance single bounce diamond ATR (attenuated total reflectance) cell. Spectra over the 4000-525 cm^{-1} range were obtained by the co-addition of 128 scans with a resolution of 4 cm^{-1} and a mirror velocity of 0.6329 m/s.

3. Results and discussion

3.1 Elemental analysis (ICP-OES)

The relationship of major ions (Al^{3+}, Mg^{2+}, Ca^{2+}, and K^{+}) present in the neutralization process are shown in Figure 2. The most noticeable trends are observed for magnesium and aluminium, which reveal an inverse relationship. The gradual decrease in aluminium confirms it is being removed from solution via the formation of a precipitate, while the absence of magnesium indicates that it is being readily used up in the formation of a precipitate. Once aluminium has been exhausted (occurs at the inflection point) the magnesium concentration starts to increase significantly, confirming the formation of hydrotalcite and the significant role that Mg^{2+} plays in the neutralization process. The

absence of aluminium in solution after the inflection point (pH) shows hydrotalcite to be stable at the end of the neutralization process.

The calcium concentration follows a similar trend to that of the magnesium-aluminium relationship discussed, except that the mechanism is caused by the formation of calcium carbonate species. The absence of calcium in solution up until the inflection point confirms that the formation of $CaCO_3$ plays a key role in the neutralization process. These results indicate that the neutralization process is controlled by the concentration of carbonate and aluminium, and once exhausted, a reduction in pH is simply a dilution effect caused by the addition of seawater or nanofiltered seawater.

3.2 Mineralogical composition

There are 4 common phases observed in the X-ray diffraction patterns (Figure 3) of all seawater and nanofiltered seawater precipitates formed between pH 13 and 9.5: hydrotalcite ($Mg_6Al(OH)_{16}CO_3{\cdot}4H_2O$), calcite ($CaCO_3$ – rhombohedra), aragonite ($CaCO_3$ – orthorhombic) and halite (NaCl). Numerous works on the seawater neutralization process has reported the formation of these phases.[7, 25-28] The formation of hydrocalumite is commonly reported, however it is not observed in this investigation. The most intense peaks are associated with the highly crystalline calcite and halite precipitates, while the very broad low intensity peaks are characteristic of hydrotalcite. High pH precipitates exhibit an additional phase, which has been determined to be $Mg_2Al(OH)_7$. The primary peak of this phase is hidden under the very broad hydrotalcite peak. However, due to the large intensity of its secondary peak, compared to the secondary peak of hydrotalcite, it can be observed at around 27° 2θ as a sharp overlapping band. This peak disappears at pH values below 11 and signifies the dissolution of the mixed metal hydroxide.

Further confirmation of the instability of $Mg_2Al(OH)_7$ is shown by a shift in intensity of the 2 water infrared deformation modes (1640 and 1585 cm^{-1}), assigned to hydrotalcite and $Mg_2Al(OH)_7$ respectively, as the pH decreases (Figure 4). At high pH, there is a significant amount of hydrogen bonding associated with $Mg_2Al(OH)_7$ (1585 cm^{-1}). As the dissolution of $Mg_2Al(OH)_7$ occurs at lower pH and hydrotalcite forms in its place, the band at 1585 cm^{-1} decreases, while the band at 1640 cm^{-1} increases confirming the formation of additional hydrotalcite after the dissolution of $Mg_2Al(OH)_7$. Hydrotalcite shares a common band at 1585 cm^{-1} due to the similarity of the bonding environment of Mg,Al-OH layers in hydrotalcite and $Mg_2Al(OH)_7$, which results in the band remaining at low pH.

Infrared spectra confirm the presence of aragonite and calcite in the precipitates with the appearance of C-O vibrational bands at 1490/1090cm^{-1} in seawater and 1410/1085cm^{-1} in NF. The corresponding bending mode of these carbonate groups are observed at 875cm^{-1}. At high pH, the shape of the band assigned to υ_3 vibrational modes of carbonate clearly shows a shoulder band at around 1410cm^{-1},

however as the pH decreases the shoulder band intensifies. Based on XRD (aragonite and calcite in all precipitates), it is believed that the increased clarity of the shoulder band at 1410cm^{-1} for the pH 9.5 precipitates is due to a smaller ratio of aragonite in the sample that allows the calcite band to be more pronounce. In the XRD patterns, precipitates collected at pH 10 show evidence of sodium sulphate (Na_2SO_4) while those at pH 12.5 do not. A similar trend is noticed for the 1110cm^{-1} band in the infrared spectra. Based on these observations it is proposed that the 1110cm^{-1} band is associated with sulphate anions in Na_2SO_4. The formation of both calcite and aragonite in seawater neutralisation conditions has been explained by a report written by Choudens-Sanchez and Gonzalez,[29] which states that the precipitation of calcite and aragonite are dependent on the saturation ratio (with respects to $CaCO_3$) and the Mg:Ca ratio in solution. During the seawater neutralisation process, the solution chemistry is constantly changing as precipitates form, in particular hydrotalcite, which results in THE formation of $CaCO_3$ at different Mg:Ca ratios. Aragonite typically forms in high Mg:Ca solutions and low supersaturation conditions due to a reduction in calcite growth caused by Mg substitution. This has been shown in XRD and IR data, whereby aragonite is more prevalent in the high pH precipitates, while calcite dominates in the low pH precipitates.

The mechanisms responsible for the neutralization process are the formation of hydrotalcite and $CaCO_3$. Carbonate alkalinity is proposed to be removed by two different mechanisms: 1) formation of $CaCO_3$ and 2) intercalation into the hydrotalcite structure. This investigation found that in the absence of Ca^{2+}, minimal changes in neutralization efficiency occurred suggesting CO_3^{2-} removal is by means of intercalation. It is also believed that in rich Ca^{2+} solutions, carbonate is predominately removed from solution via the formation of $CaCO_3$, which then allows sulphate anions to be intercalated into the hydrotalcite structure due to reduced competition for interlayer sites.

3.3 Conductivity

The conductivity of the seawater and nanofiltered seawater neutralization shows multiple steps occurring that were not identifiable by pH measurements alone (Supporting Information 3). The rapid decline in conductivity at the beginning of the curve (up to 30mL of seawater) is believed to be primarily due to the decrease in NaOH (contributes significantly to conductivity values) as hydrotalcite and $Mg_2Al(OH)_7$ forms (Equations 1-3):

Equation 1: Hydrotalcite (2:1) formation

$$\mathbf{4NaOH}_{(aq)} + 4MgCl_2{\cdot}6H_2O_{(aq)} + 2NaAl(OH)_{4(aq)} + Na_2CO_{3(aq)} \rightarrow \mathbf{Mg_4Al_2(OH)_{12}(CO_3){\cdot}4H_2O_{(s)}} + 8NaCl_{(aq)} + 2H_2O_{(l)}$$

Equation 2: Hydrotalcite (3:1) formation

$$\mathbf{8NaOH}_{(aq)} + 6MgCl_2{\cdot}6H_2O_{(aq)} + 2NaAl(OH)_{4(aq)} + Na_2CO_{3(aq)} \rightarrow \mathbf{Mg_6Al_2(OH)_{16}(CO_3){\cdot}4H_2O_{(s)}} + 12NaCl_{(aq)} + 2H_2O_{(l)}$$

Equation 3: $Mg_2Al(OH)_7$ formation

$$\mathbf{3NaOH}_{(aq)} + 2MgCl_2 \cdot 6H_2O_{(aq)} + NaAl(OH)_{4(aq)} \rightarrow \mathbf{Mg_2Al(OH)_{7(s)}} + 4NaCl_{(aq)} + 6H_2O_{(l)}$$

In contrast, the slow and steady decrease in pH at the beginning of the neutralization process indicates a buffering agent, such as carbonate, is slowing the rate of neutralization. Even though $CaCO_3$ is shown to form during the initial stage of neutralization, it's not until the rate of $Mg_2Al(OH)_7$ and hydrotalcite formation reduces that the removal of carbonate alkalinity is observed as a rapid decrease in pH (Equation 4).

Equation 4: Formation of $CaCO_3$ (calcite / aragonite)

$$\mathbf{Na_2CO_{3(aq)}} + CaCl_2 \cdot 6H_2O_{(aq)} \rightarrow \mathbf{CaCO_{3(s)}} + 2NaCl_{(aq)} + 6H_2O_{(l)}$$

Both the seawater and nanofiltered seawater conductivity curves show a number of fluctuations corresponding to the inflection point on the pH curve. These fluctuations are believed to be associated with multiple reactions involved with the dissolution of $Mg_2Al(OH)_7$, the formation of additional hydrotalcite and $CaCO_3$ facilitated by the dissolution products, and ion exchange reactions. Based on excess calcium remaining in solution at the end of the neutralization process, it is believed that the majority of carbonate has been removed from solution, and as a result the newly formed hydrotalcite has predominantly sulphate anions intercalated between the hydroxide layers. After the inflection point (pH), the conductivity slowly increases due to NaCl and other ions in seawater that are no longer reacting to form precipitates.

3.4 Efficiency of neutralization

The differences in neutralization efficiency for different Mg^{2+} sources are clearly shown in Figure 5, with the nanofiltered seawater sources (real and synthetic) increasing the overall efficiency of neutralization by approximately 50% (about 2.3 times quicker for both Bayer liquors). This increase in efficiency is essentially proportional to the increased concentration of Mg^{2+} and Ca^{2+} ions (combined increase is 2.2). The neutralization efficiency appears to follow pseudo-first order kinetics, however the actual rate law is significantly more complex involving multiple formation, dissolution and ion exchange reactions.

Comparison of the curves based on mol/L Mg^{2+} added (Figure 5) shows that there is only a small variation in pH obtained for solutions with a lower cation content (increased cation concentration equates to an increased neutralization efficiency). Therefore, the neutralization process is proportional to the total concentration of cations used up in the formation of OH^- and CO_3^{2-} compounds, with Mg^{2+} precipitates having the greatest neutralization capacity. The fact that the curves are very similar

suggests that similar neutralization mechanisms are occurring independent of initial cation concentration effects.

The concentration of reacted Al^{3+}, Mg^{2+} and Ca^{2+} during the neutralization process and the corresponding percentage of those ions used in the formation of precipitates can be found in Table 1. Results indicate that hydrotalcite forms a combination of 2:1 and 3:1 hydrotalcite structures (Equations 1 and 2, respectively). The formation of $Mg_2Al(OH)_7$ at high pH will influence the Mg:Al ratio, however after the dissolution of $Mg_2Al(OH)_7$ at pH 11, the Mg:Al ratio should give an indication on the type of hydrotalcite that forms. The nanofiltered molar ratio is smaller than seawater (2.2 compared to 2.9) and indicates that a large Mg^{2+} concentration in the initial stages of neutralization favours the 2:1 hydrotalcite.

The infrared spectra provide additional information on the Mg:Al ratio of the precipitates that form (Figure 4). The intense infrared band situated at 1365 cm^{-1} is due to the ν_3 vibrational mode of carbonate in the hydrotalcite interlayer. The position of the band suggests that hydrotalcite has an Mg:Al ratio of 3:1.[30-32] However, the precipitates at pH 12 and 13 show a small shoulder at 1340 cm^{-1} indicative of a 2:1 hydrotalcite structure. This suggests that a mixture of hydrotalcite structures form, with the 3:1 being the most abundant at the end of the neutralization process.

3.5 Comparison of nanofiltered seawater and seawater

Alternative seawater sources for the seawater neutralization of alumina wastewater have the potential to improve the waste management program currently adopted by participating refineries based on a number of environmental, social and economic issues. As the cost of production increases, due to lower grade bauxite ore being processed, it is necessary to find more affordable and environmentally friendly alternatives to ensure the sustainability of the industry. The greatest economic value in using nanofiltered seawater is the reduced volume required to achieve the same degree of neutralization. Currently, large amounts of seawater are required (15 to 20 times the volume of red mud to be neutralized) to achieve the environmental standards required for red mud to be safely disposed in tailing dams, while the magnesium and calcium depleted seawater is discharged back to sea.[33] The doubling of magnesium and calcium in nanofiltered seawater results in an approximate 50% reduction in volume required to achieve the same neutralization capacity as seawater. Thus, it increases the neutralizing capacity per volume of neutralizing reagent.

These reductions in time and volume translate into increased productivity. Each alumina refinery has unique operating and cost structures and it is acknowledged that the capital cost for NF seawater will be higher than direct feed seawater plants, however in a greenfield development significant savings are possible through reduced sizing of downstream residue infrastructure and footprint, as well as reduced power associated with pumping costs. For a brownfield expansion to existing plants, upstream processing capacity can be increased without the need to proportionally increase the footprint and infrastructure associated with the tailings circuit, such as piping, reaction vessels, thickeners and clarifiers, as well as the associated costs of pumping throughout the plant and discharge.

The installation of a nanofiltered plant onsite is the only new investment required, however the advantages of using nanofiltered seawater could offset these initial implementation costs in higher volume refineries already using the seawater neutralisation process. The capital costs can be further reduced if a desalination plant is located within the vicinity of the alumina refinery and the two industries operate synergistically by sharing in the capital investment and the alumina refinery receiving the desalination plant's brine discharge stream. The total economic advantages is case specific, however it is proposed that the majority of alumina refineries using the seawater neutralization process would benefit from the implementation of this technology. The report by Taylor et. al.,[24] provides more detail on the economic advantages of using membrane technology in the seawater neutralization process.

Apart from the visible effects of tailings on the landscape, the major ecological impact of industry is water pollution arising from discharge that causes adverse effects in aquatic ecosystems. Determining the eventual fate and effect of tailings discharge in coastal environments and biota is a highly dynamic proposition that requires interdisciplinary evaluation, however reducing the amount of discharge is always going to improve/minimize environmental impacts.

Conclusions

This investigation has shown that the reaction mechanisms responsible for the neutralization of alumina wastewater are highly similar for all seawater sources, with only minor variations in hydrotalcite and calcium carbonate crystal structures being observed. These changes do not appear to have any significant influence on the overall stability of the neutralization precipitates during or at the end of the neutralization process. XRD data indicates the presence of hydrotalcite, calcite, aragonite and halite as the major mineralogical phases involved in the process, with $Mg_2Al(OH)_7$ also observed above pH 12.5. Various fluctuations in conductivity measurements throughout the neutralization process indicate that a number of dissolution/formation steps are occurring. Another important finding is the appearance of a direct correlation between the concentration of magnesium and calcium on the

362 efficiency of the neutralization process. This investigation has determined that a number of reactions
363 are responsible for the overall neutralization process; however estimations can be made about
364 neutralization efficiency using the magnesium and calcium concentration.
365
366 Hydrotalcite undergoes a number of reactions, with the most significant being: 1) ion exchange of
367 interlayer anions, 2) rearrangement of the hydroxide layers, and 3) substitution of Mg^{2+} into the
368 hydroxide layer as the pH decreases. All of these reactions are outlined in Figure 6. The formation of
369 hydrotalcite is facilitated by: 1) excess Mg^{2+} (seawater), $Al(OH)_4^-$ and NaOH (Bayer liquor), and 2)
370 the dissolution of $Mg_2Al(OH)_7$.
371
372 This investigation has shown that the reaction mechanisms responsible for the neutralization of
373 alumina wastewater are highly similar for seawater and nanofiltered seawater, with only minor
374 variations in hydrotalcite and calcium carbonate crystal structures being observed. These changes do
375 not appear to have any significant influence on the overall stability of the neutralization precipitates
376 during or at the end of the neutralization process. Another important finding is the appearance of a
377 direct correlation between the concentration of magnesium and calcium on the efficiency of
378 neutralization, which appears to follow pseudo-first order reaction kinetics (based on the combined
379 effect of magnesium and calcium). This in-depth investigation has determined that a number of
380 reactions are responsible for the overall neutralization process; however estimations can be made
381 using the magnesium and calcium concentration. It has also been shown that the formation of calcium
382 carbonate has a significant role in the intercalation of sulphate anions in the hydrotalcite interlayer.
383 The similarity of results confirms that the use of nanofiltered seawater can be used in current
384 applications that use seawater neutralized residue but with the added advantages of reduced volumes
385 and salt content.
386
387 **Acknowledgements**
388 The financial and infra-structure support of the Energy and Process Engineering Discipline of
389 the Science and Engineering Faculty and the Institute of Future Environments, Queensland
390 University of Technology is gratefully acknowledged. The Australian Research Council
391 (ARC) is thanked for funding some of the instrumentation used in this study (DE120101890).
392 This study could also not have been completed without the support of the technical services
393 team at QUT who ensured the analytical instrumentation was available to us.
394

References

1. Hind, A. R.; Bhargava, S. K.; Grocott, S. C., The surface chemistry of Bayer process solids: a review. *Colloids Surf., A* **1999,** *146*, (1-3), 359-374.
2. Oeberg, N. C. R.; Steinlechner, E. H., Red mud and sands handling new thoughts on an old problem. *Light Met. (Warrendale, Pa.)* **1996**, 67-73.
3. Power, G.; Graefe, M.; Klauber, C., Bauxite residue issues: I. Current management, disposal and storage practices. *Hydrometallurgy* **2011,** *108*, (1-2), 33-45.
4. Basal Convention. Basel Convention on the Control of Transboundary Movements of Hazardous Wastes and Their Disposal, *United Nations Environment Programme*, 2011.
5. Brecht, P., Mud, glorious mud. *Nurs Stand* **1997,** *11*, 20-1.
6. Maddocks, G.; Lin, C.; McConchie, D., Field scale remediation of mine wastes at an abandoned gold mine, Australia II: Effects on plant growth and groundwater. *Environ. Geol. (Heidelberg, Ger.)* **2009,** *57*, 987-996.
7. Menzies, N. W.; Fulton, I. M.; Morrell, W. J., Seawater Neutralization of Alkaline Bauxite Residue and Implications for Revegetation. *Journal of Environmental Quality* **2004,** *33*, (5), 1877-84.
8. Zhang, L.; Feng, X.; Xiao, B., Research progresses in application of red mud to environmental pollution treatment. *Huagong Huanbao* **2010,** *30*, (1), 34-37.
9. Jones, B. E. H.; Haynes, R. J., Bauxite Processing Residue: A Critical Review of Its Formation, Properties, Storage, and Revegetation. *Crit. Rev. Environ. Sci. Technol.* **2011,** *41*, 271-315.
10. Zhou, Y.-F.; Haynes, R. J., A Comparison of Water Treatment Sludge and Red Mud as Adsorbents of As and Se in Aqueous Solution and Their Capacity for Desorption and Regeneration. *Water, Air, Soil Pollut.* **2012,** *223*, (9), 5563-5573.
11. Zhao, Y.; Yue, Q.; Li, Q.; Xu, X.; Yang, Z.; Wang, X.; Gao, B.; Yu, H., Characterization of red mud granular adsorbent (RMGA) and its performance on phosphate removal from aqueous solution. *Chem. Eng. J. (Amsterdam, Neth.)* **2012,** *193-194*, 161-168.
12. Burkov, K. A.; Karavan, S. V.; Pinchuk, O. A., Red mud for purification of galvanic wastewater. *Russ. J. Appl. Chem.* **2012,** *85*, (12), 1838-1844.
13. Ali, I.; Asim, M.; Khan, T. A., Low cost adsorbents for the removal of organic pollutants from wastewater. *J. Environ. Manage.* **2012,** *113*, 170-183.
14. Ahmaruzzaman, M., Industrial wastes as low-cost potential adsorbents for the treatment of wastewater laden with heavy metals. *Adv. Colloid Interface Sci.* **2011,** *166*, (1-2), 36-59.
15. Zou, J.; Ruan, Z. Method for recovery and utilization of red mud. CN102531440A, 2012.
16. Thakur, R. S.; Sant, B. R., Utilization of red mud: Part II - Recovery of alkali, iron, aluminum, titanium and other constituents and the pollution problems. *J. Sci. Ind. Res.* **1983,** *42*, (8), 456-69.
17. Zimmer, E., Process for the utilization of red mud as a secondary raw material source. *Aluminium (Duesseldorf)* **1980,** *56*, (10), 639-42.
18. McConchie, D.; The use of seawater-neutralized bauxite refinery residues (red mud) in environmental remediation programs. *Proceedings of the "Rewas'99 Global Symposium on Recycling, Waste Treatment and Clean Technology"*, San Sebastian, Spain, September 5-9, 1999.
19. Johnston, M.; Clark, M. W.; McMahon, P.; Ward, N., Alkalinity conversion of bauxite refinery residues by neutralization. *J. Hazard. Mater.* **2010,** *182*, 710-715.
20. Department of Environment and Heritage Protection, Wastewater release to Queensland waters, Environmental Protection Act 1994.
21. Smith, H. D.; Parkinson, G. M.; Hart, R. D., In situ absorption of molybdate and vanadate during precipitation of hydrotalcite from sodium aluminate solutions. *J. Cryst. Growth* **2005,** *275*, (1-2), 1665-1671.
22. Kennish, M. J., Trace metal-sediment dynamics in estuaries: Pollution assessment. *Rev. Environ. Contam. Toxicol.* **1998,** *155*, 69-110.

23. Bengtsson, B. E., Biological variables, especially skeletal deformities in fish, for monitoring marine pollution. *Philos Trans R Soc Lond B Biol Sci* **1979,** *286*, (1015), 457-64.
24. Taylor, K.; Mullett, M.; Fergusson, L.; Adamson, H.; Wehrli, J., Application of nanofiltration technology to improve sea water neutralization of Bayer process residue. *Light Met. (Hoboken, NJ, U. S.)* **2011**, 81-87.
25. Genc-Fuhrman, H.; Tjell, J. C.; McConchie, D., Increasing the arsenate adsorption capacity of neutralized red mud (Bauxsol). *J. Colloid Interface Sci.* **2004,** *271*, 313-320.
26. Hanahan, C.; McConchie, D.; Pohl, J.; Creelman, R.; Clark, M.; Stocksiek, C., Chemistry of Seawater Neutralization of Bauxite Refinery Residues (Red Mud). *Environ. Eng. Sci.* **2004,** *21*, 125-138.
27. McConchie, D.; Clark, M.; Hanahan, C.; Fawkes, R. In *The use of seawater-neutralized bauxite refinery residues (red mud) in environmental remediation programs*, 1999; Minerals, Metals & Materials Society: 1999; pp 391-400.
28. McConchie, D.; Saenger, P.; Fawkes, R. In *An environmental assessment of the use of seawater to neutralize bauxite refinery wastes*, 1996; Minerals, Metals & Materials Society: 1996; pp 407-416.
29. De, C.-S. V.; Gonzalez, L. A., Calcite and aragonite precipitation under controlled instantaneous supersaturation: elucidating the role of CaCO3 saturation state and Mg/Ca ratio on calcium carbonate polymorphism. *J. Sediment. Res.* **2009,** *79*, 363-376.
30. Farmer, V. C.; Editor, *Mineralogical Society Monograph 4: The Infrared Spectra of Minerals*. Mineral. Soc.: 1974; p 539 pp.
31. Palmer, S. J.; Frost, R. L.; Nguyen, T., Hydrotalcites and their role in coordination of anions in Bayer liquors: Anion binding in layered double hydroxides. *Coord. Chem. Rev.* **2009,** *253*, 250-267.
32. Xu, Z. P.; Zhang, J.; Adebajo, M. O.; Zhang, H.; Zhou, C., Catalytic applications of layered double hydroxides and derivatives. *Appl. Clay Sci.* **2011,** *53*, 139-150.
33. Anon, Red menace-alumina waste products neutralized. *Mater. World* **2003,** *11*, (6), 22-24.

List of tables

List of figures

497 **Table 1**

Seawater							
pH	Reacted Al		Reacted Mg		Mg:Al	Reacted Ca	
	mg/L	%	mg/L	%		mg/L	%
	2433.0	-	**1411.5**	-		**446.0**	-
13.05	310.5	28.1	752.6	97.8	**2.69**	237.3	97.5
12.53	475.1	74.2	1034.8	99.5	**2.42**	326.7	99.4
11.5	474.2	99.0	1129.2	99.6	**2.64**	350.7	97.9
11.14	454.2	99.3	1139.9	99.5	**2.79**	352.1	97.2
10.51	440.3	99.2	1141.9	99.0	**2.88**	348.7	95.6
9.52	390.5	99.5	1069.3	90.3	**3.04**	291.6	77.9
Nanofiltered seawater							
pH	Reacted Al		Reacted Mg		Mg:Al	Reacted Ca	
	mg/L	%	mg/L	%		mg/L	%
	2433.0	-	**3141.5**	-		**956.0**	-
12.99	419.9	24.2	717.6	79.9	**1.90**	93.1	34.1
12.51	865.8	78.3	1425.3	83.2	**1.83**	233.3	44.7
11.62	878.6	99.7	1671.5	83.4	**2.11**	277.8	45.6
10.95	854.8	99.8	1709.9	84.0	**2.22**	294.0	47.5
10.37	842.0	99.7	1719.6	83.9	**2.27**	293.0	46.9
9.42	808.5	99.7	1765.5	84.3	**2.42**	308.5	48.4

498

499

500 **Figure 1**

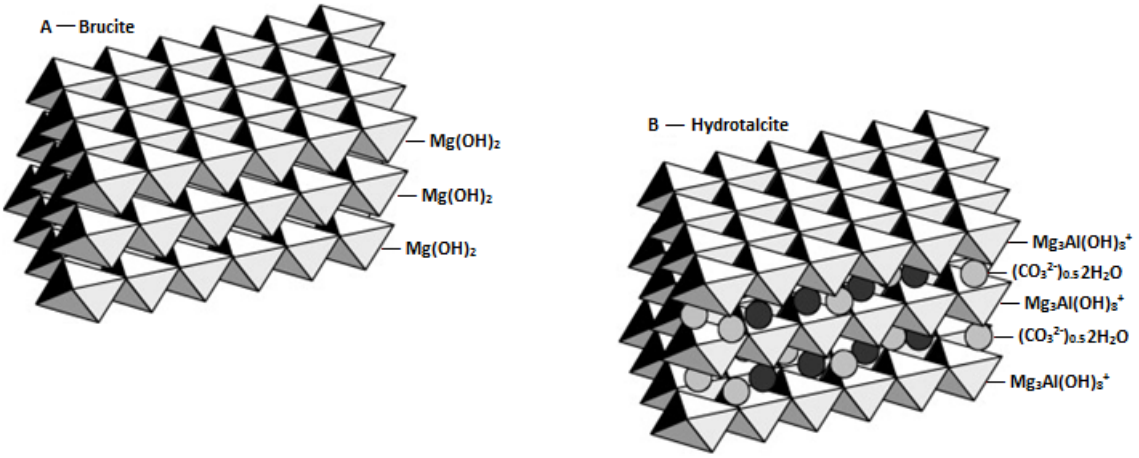

501

502

503

Figure 2

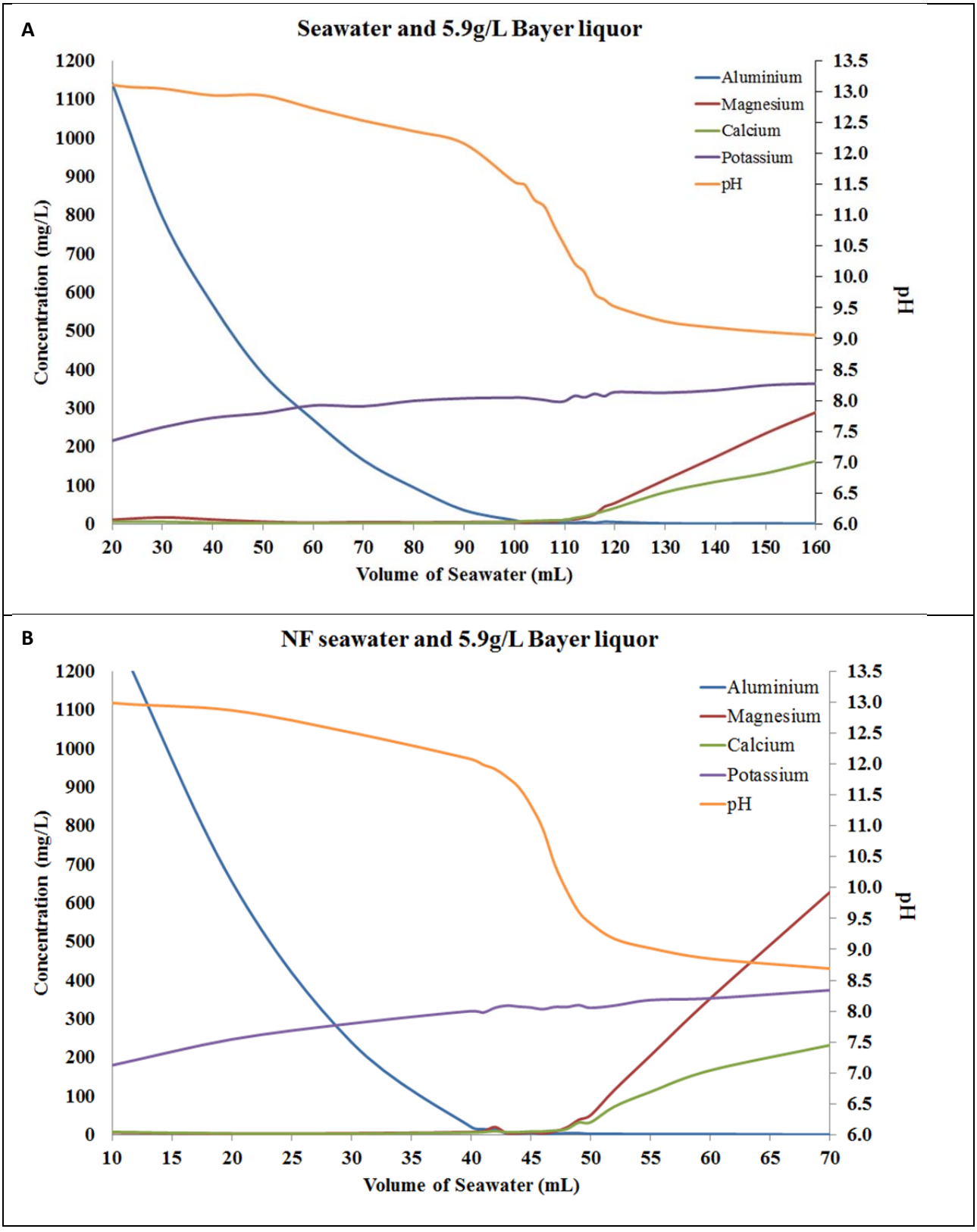
A
Seawater and 5.9g/L Bayer liquor
Aluminium
Magnesium
Calcium
Potassium
pH
Concentration (mg/L)
pH
Volume of Seawater (mL)
B
NF seawater and 5.9g/L Bayer liquor
Aluminium
Magnesium
Calcium
Potassium
pH
Concentration (mg/L)
pH
Volume of Seawater (mL)

508 **Figure 3**

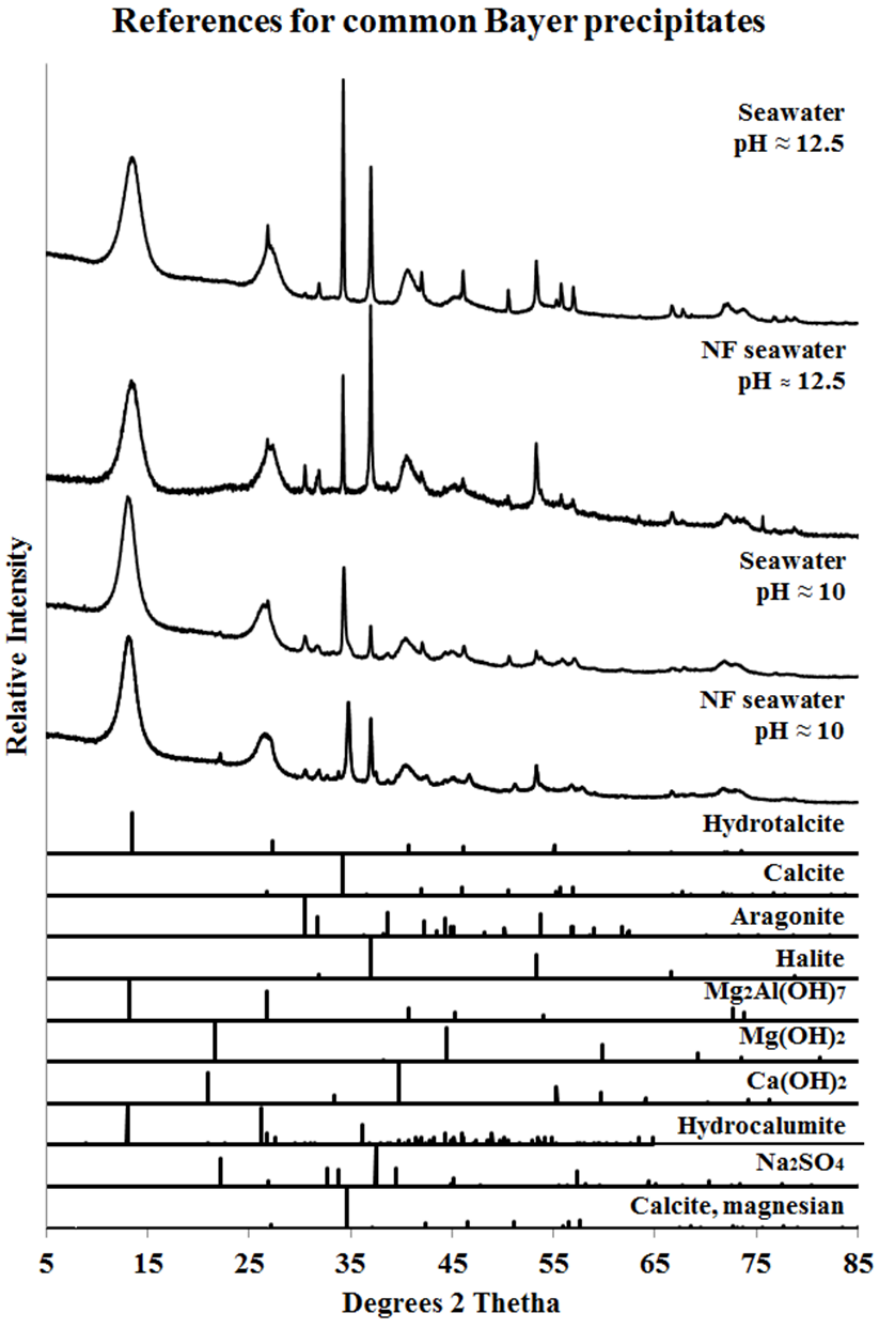

509

510

511

512 **Figure 4**

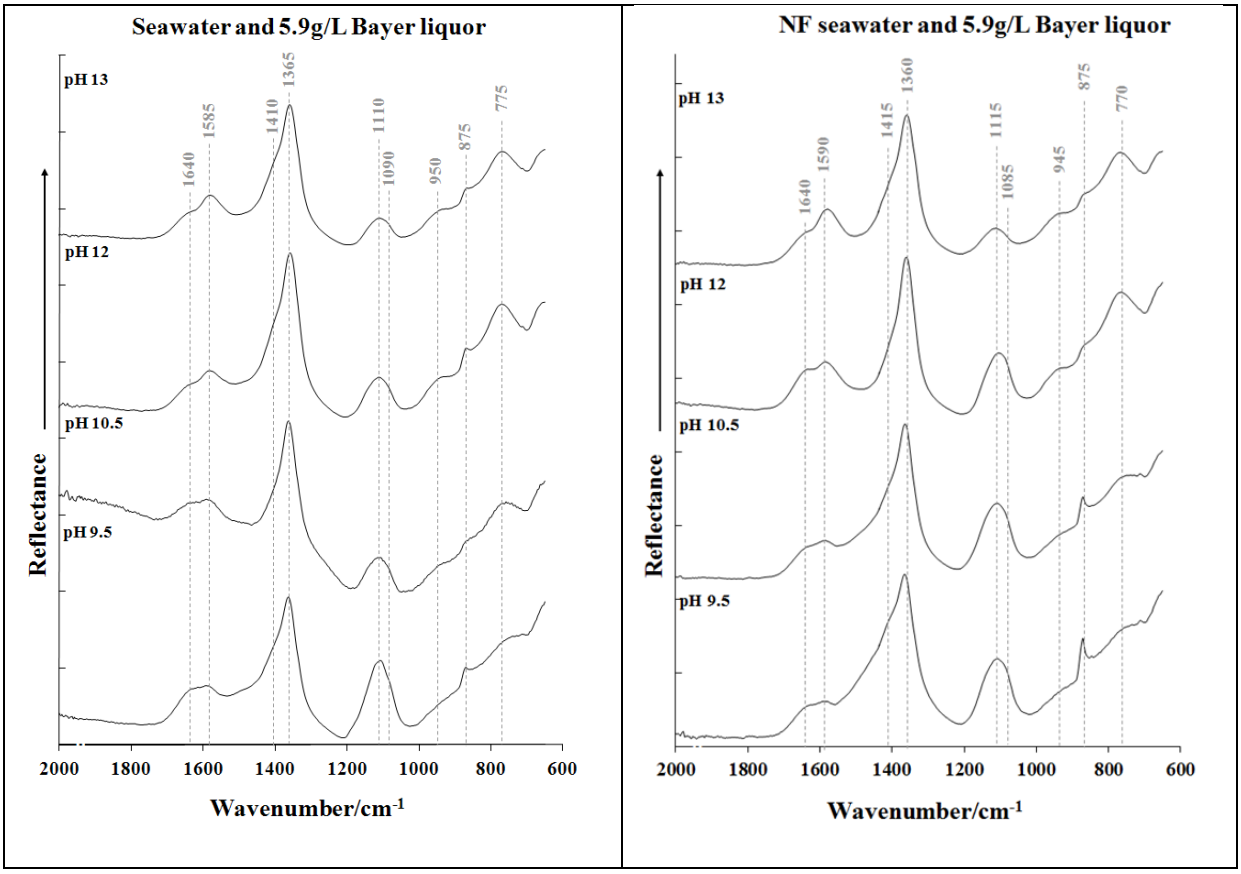

513

Figure 5

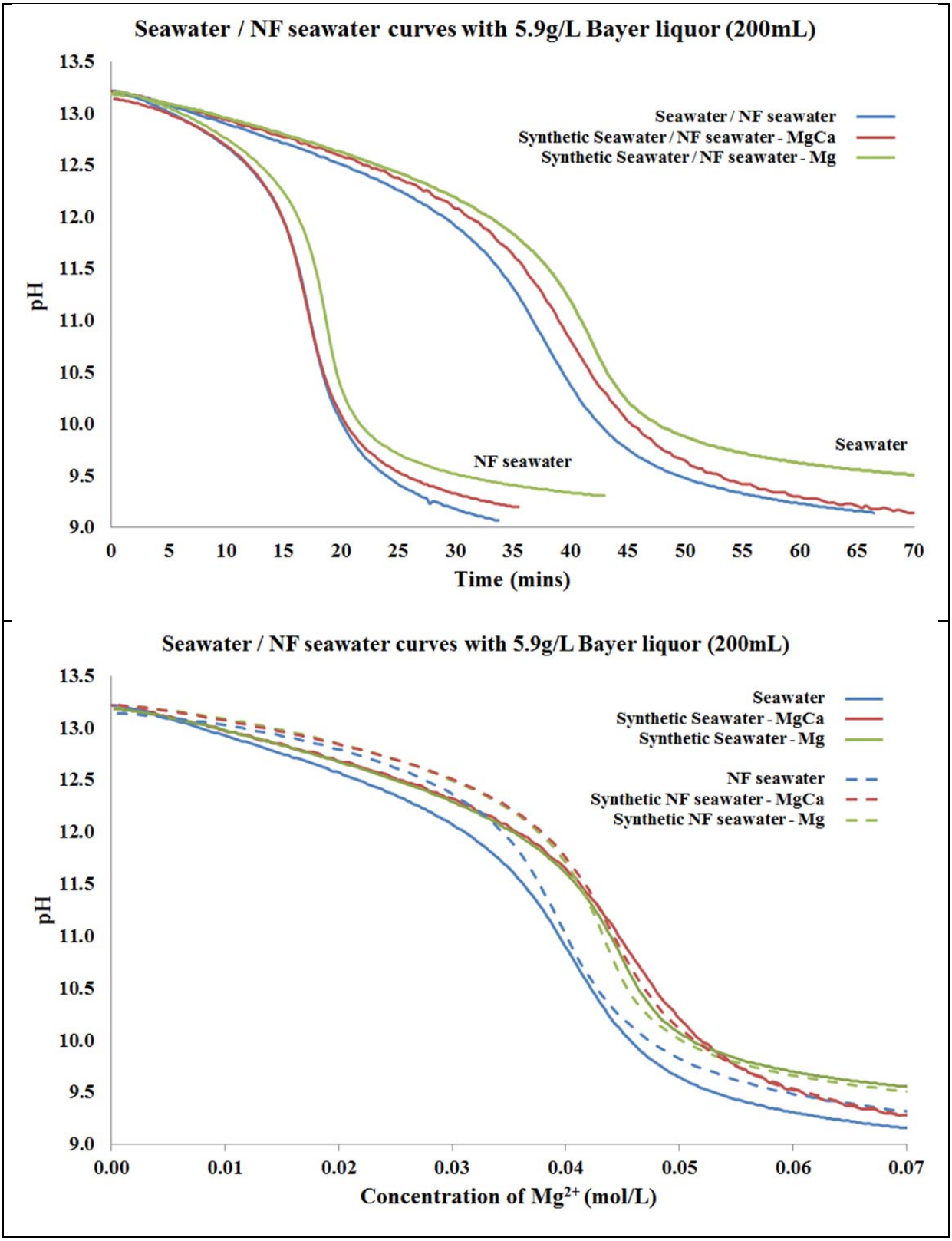
Seawater / NF seawater curves with 5.9g/L Bayer liquor (200mL)
pH
Time (mins)
Seawater / NF seawater
Synthetic Seawater / NF seawater - MgCa
Synthetic Seawater / NF seawater - Mg
NF seawater
Seawater
Seawater / NF seawater curves with 5.9g/L Bayer liquor (200mL)
pH
Concentration of Mg2+ (mol/L)
Seawater
Synthetic Seawater - MgCa
Synthetic Seawater - Mg
NF seawater
Synthetic NF seawater - MgCa
Synthetic NF seawater - Mg

Figure 6

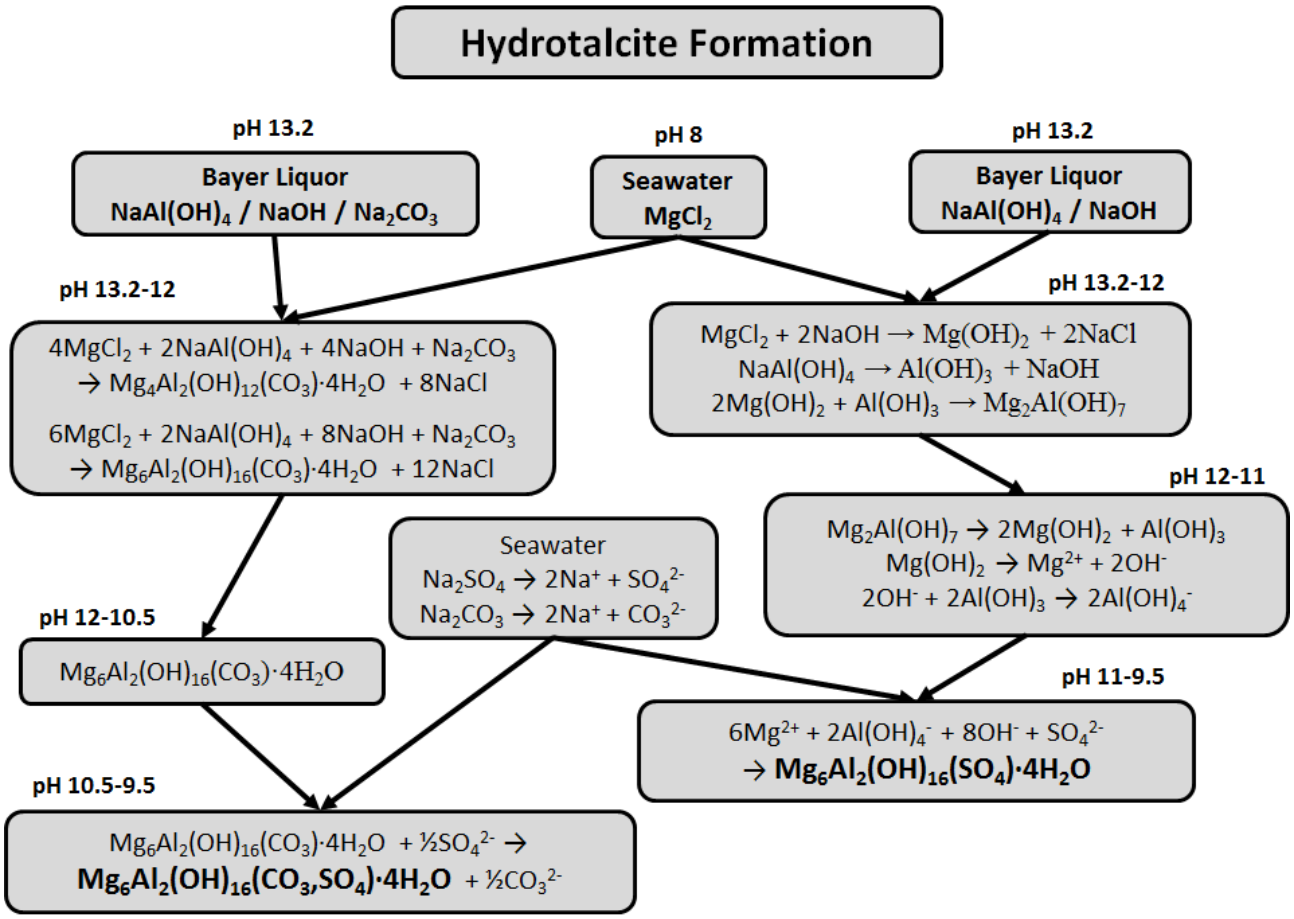
Hydrotalcite Formation
pH 13.2
Bayer Liquor
NaAl(OH)4 / NaOH / Na2CO3
pH 8
Seawater
MgCl2
pH 13.2
Bayer Liquor
NaAl(OH)4 / NaOH
pH 13.2-12
4MgCl2 + 2NaAl(OH)4 + 4NaOH + Na2CO3
→ Mg4Al2(OH)12(CO3)·4H2O + 8NaCl
6MgCl2 + 2NaAl(OH)4 + 8NaOH + Na2CO3
→ Mg6Al2(OH)16(CO3)·4H2O + 12NaCl
pH 13.2-12
MgCl2 + 2NaOH → Mg(OH)2 + 2NaCl
NaAl(OH)4 → Al(OH)3 + NaOH
2Mg(OH)2 + Al(OH)3 → Mg2Al(OH)7
pH 12-11
Mg2Al(OH)7 → 2Mg(OH)2 + Al(OH)3
Mg(OH)2 → Mg2+ + 2OH-
2OH- + 2Al(OH)3 → 2Al(OH)4-
Seawater
Na2SO4 → 2Na+ + SO42-
Na2CO3 → 2Na+ + CO32-
pH 12-10.5
Mg6Al2(OH)16(CO3)·4H2O
pH 11-9.5
6Mg2+ + 2Al(OH)4- + 8OH- + SO42-
→ Mg6Al2(OH)16(SO4)·4H2O
pH 10.5-9.5
Mg6Al2(OH)16(CO3)·4H2O + ½SO42- →
Mg6Al2(OH)16(CO3,SO4)·4H2O + ½CO32-